Far-infrared optical excitations in multiferroic $TbMnO_3$

M. Schmidt[1,a], Ch. Kant[1], T. Rudolf[1], F. Mayr[1], A.A. Mukhin[2], A.M. Balbashov[3], J. Deisenhofer[1], and A. Loidl[1]

[1] Experimental Physics V, Center for Electronic Correlations and Magnetism, University of Augsburg, 86135 Augsburg, Germany
[2] General Physics Institute of the Russian Academy of Sciences, 119991 Moscow, Russia
[3] Moscow Power Engineering Institute, 105835 Moscow, Russia

Abstract. We provide a detailed study of the reflectivity of multiferroic $TbMnO_3$ for wave numbers from 40 cm^{-1} to 1000 cm^{-1} and temperatures 5 K $< T <$ 300 K. Excitations are studied for polarization directions $\mathbf{E} \parallel \mathbf{a}$, the polarization where electromagnons are observed, and for $\mathbf{E} \parallel \mathbf{c}$, the direction of the spontaneous polarization in this material. The temperature dependencies of eigenfrequencies, damping constants and polar strengths of all modes are studied and analyzed. For $\mathbf{E} \parallel \mathbf{a}$ and below the spiral ordering temperature of about 27 K we observe a transfer of optical weight from phonon excitations to electromagnons, which mainly involves low-frequency phonons. For $\mathbf{E} \parallel \mathbf{c}$ an unusual increase of the total polar strength and hence of the dielectric constant is observed indicating significant transfer of dynamic charge probably within manganese-oxygen bonds on decreasing temperatures.

PACS. 63.20.kk Phonon interactions with other quasiparticles – 63.20.-e Phonons in crystal lattices – 75.47.Lx Manganites – 78.30.-j Infrared and Raman spectra

1 Introduction

The discovery of spin-driven ferroelectricity in some rare earth manganites [1] has revived the field of multiferroics enormously [2–4]. In these systems the onset of ferroelectricity is directly coupled to the static non-collinear spin order [5–7]. Concerning the dynamics of multiferroics, the idea of hybridization between spin waves and optical phonons in magnetoelectrics has been put forth long ago by Smolenskii and Chupis [8], and indeed, ample experimental evidence for the occurrence of electromagnons in the rare earth manganites has been provided recently [9–14]. The origin and the underlying mechanisms of these magnetoelectric excitations have been debated vividly [15,16], however, recent studies [17,18] support the scenario that magnons in spin-driven ferroelectrics can gain optical weight via the coupling to phonons and, hence, can be observed directly in far-infrared (FIR) and THz spectroscopy. A strong correlation of electromagnons and phonons has been already reported for the case of $GdMnO_3$ as function of temperature and magnetic field [19].

$TbMnO_3$ is by far the most studied multiferroic manganite and crystallizes in an orthorhombically distorted perovskite structure (space group *Pbnm*). It reveals magnetic phase transitions into an antiferromagnetic (AFM) collinear spin structure at $T_N = 42$ K and subsequently in a structure with helical spin order and spontaneous ferroelectric (FE) polarization at $T_{FE} = 27$ K [1]. In the low temperature structure the spins reveal helicoidal order with a propagation vector along the crystallographic **b** direction and the spin spiral plane lying within the bc plane [20]. In this case the FE polarization is expected to be along the **c** direction [6,21] in agreement with experiment [1]. In $TbMnO_3$ electromagnons have been observed at wave numbers close to 20 cm^{-1} [9,17,18] and 60 cm^{-1} [17], which exactly matches spin wave dispersion energies as determined in neutron scattering experiments [22,23].

For the low-energy electromagnon the optical eigenfrequency corresponds to the new magnetic Bragg point at (0, 0.28, 1) and the magnetoelectric excitation at 60 cm^{-1} matches the magnon energy at the magnetic-zone boundary [17,22,23]. Recently it has been argued that this range of electromagnons strongly overlaps with a continuum band of two-magnon absorption [15,16]. It seems, however, that the two-magnon scattering is too weak to explain the experimentally observed electromagnon intensities [17]. For the low frequency mode, it has been clearly documented in optical experiments using THz spectroscopy that the observed electromagnon eigenfrequencies correspond to spin waves, as AFM resonance absorptions have been detected using different excitation geometries in the same frequency range [18]. In $TbMnO_3$ it also became clear that the electromagnons only appear for $\mathbf{E} \parallel \mathbf{a}$ and are strictly tied to the lattice. Furthermore it has been shown that Heisenberg coupling is very important [17] and that the dynamical magnetoelectric effect as proposed by

[a] e-mail: michael.schmidt@physik.uni-augsburg.de

Katsura, Nagaosa and Balatsky cannot play a dominant role in $TbMnO_3$ [21].

The aim of this work is to investigate the temperature dependence of all infrared active phonon modes in $TbMnO_3$ in order to reveal the coupling of phonons and spin waves and to analyze the transfer of optical spectral weight at the onset of the spiral-spin order.

2 Experimental details

The investigated single crystals have previously been used for studies in the THz frequency range [9,18]. The samples were characterized by X-ray, magnetic, thermodynamic and dielectric measurements and exhibited good agreement with published results [1,24]. The optical experiments were carried out using Bruker Fourier transform spectrometers IFS 113 v and IFS 66 v/S equipped with a He-flow cryostat for wave numbers from 40 cm^{-1} to 32 000 cm^{-1} and for temperatures from 5 K to room temperature. The measurements were performed for light polarized parallel to the crystallographic **c** axis (**E** ∥ **c**), the direction of the FE polarization, and for **E** ∥ **a**, the polarization where electromagnons are observable.

The reflectivity spectra obtained at 6 K and 295 K for **E** ∥ **a** and **E** ∥ **c** are shown in Figures 1a and 1b, respectively. The reflectivity has been fitted with RefFIT [25], using a sum of Lorentzian oscillators with eigenfrequency, damping and dielectric strength as relevant fitting parameters [26].

The eigenfrequencies correspond to the transverse optical phonon modes and the longitudinal mode frequencies have to be calculated via the Lyddane-Sachs Teller relation. From the dielectric strength the effective ionic plasma frequencies can be determined, which allows some conclusions concerning the effective dynamic charges involved in specific modes [27].

For clarity in some cases we also show the frequency dependence of the dielectric loss. The complex dielectric constant has been derived from the reflectivity spectra by means of Kramers-Kronig transformation with a constant extrapolation towards low frequencies and a smooth ω^n high-frequency extrapolation.

The inset of Figure 1 shows the reflectivity of $TbMnO_3$ with **E** ∥ **a** at room temperature as measured up to 32 000 cm^{-1} (≈4 eV). The hump close to 16 000 cm^{-1} probably corresponds to dipole forbidden onsite transitions within the d multiplet of the manganese ions [28–30]. The charge transfer gap appears close to 24 000 cm^{-1}, corresponding to 3 eV. The analysis of these electronic transitions will not be subject of this work. In the present work the high-energy reflectivity is merely used to determine the electronic dielectric constant ϵ_∞ with high accuracy.

3 Experimental results and discussion

In the orthorhombic perovskite structure of $TbMnO_3$ (space group $Pbnm$) one expects a total of 25 IR active

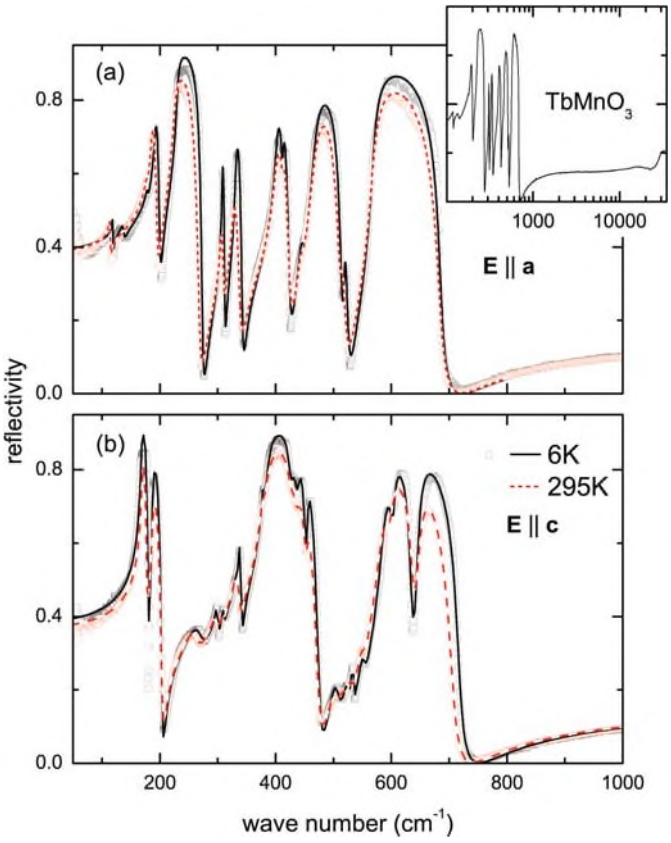

Fig. 1. (Color online) Reflectivity of $TbMnO_3$ at 295 K (open red circles) and 6 K (open black squares) for **E** ∥ **a** (upper frame) and **E** ∥ **c** (lower frame). The inset shows the experimentally observed reflectivity up to 32 000 cm^{-1} for **E** ∥ **a** at room temperature. The corresponding fit curves are shown as red dashed lines for 295 K and black solid lines at 6 K.

modes, namely 9 B_{3u} for **E** ∥ **a**, 9 B_{2u} modes for **E** ∥ **b** and 7 B_{1u} modes for **E** ∥ **c**. However, when fitting the reflectivity spectra we used 14 modes to describe the spectra for **E** ∥ **a** and 19 modes for **E** ∥ **c**. The corresponding fits describe the data nicely and are shown in Figure 1.

To identify the main IR active modes we plot the optical conductivity in Figure 2a (**E** ∥ **a**) and Figure 2b (**E** ∥ **c**) for temperatures at 6 K (solid lines) and 295 K (dashed lines). In these figures we assigned the modes with the largest optical spectral weight to the expected modes $B_{3u}(i)$ $(i = 1, ..., 9)$ and $B_{1u}(j)$ $(j = 1, ..., 7)$ for the $Pbnm$ symmetry. The additional weak modes which are visible are thought to originate from phonon modes allowed for light polarized along one of the other crystallographic axis due to polarization leakage or a slight misorientation of the sample.

The weak excitations labeled M_1 and M_2 which appear only for **E** ∥ **a** are related with the appearance of multiferroicity in this system and, hence, we will now first focus on the FIR spectra for this polarization direction.

The overall temperature dependence of the FIR spectrum for **E** ∥ **a** is illustrated in a contour plot of the dielectric loss ϵ'' as a function of temperature and wave number (see Fig. 3). In this representation all phonon modes

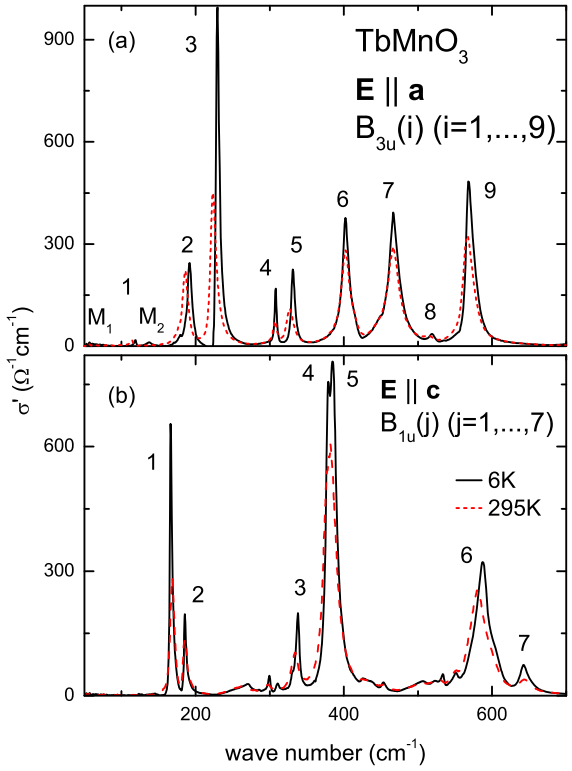

Fig. 2. (Color online) Optical conductivity of $TbMnO_3$ at 295 K (red dashed line) and 6 K (black solid line) for **E** ∥ **a** (a: upper frame) and **E** ∥ **c** (b: lower frame).

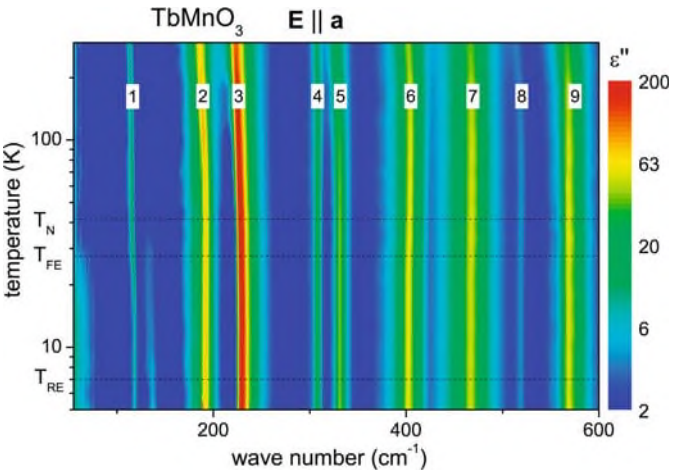

Fig. 3. (Color online) Color coded contour plot of the dielectric loss as function of temperature vs. wave number in $TbMnO_3$ for **E** ∥ **a**. Strong loss contributions are indicated in red. The color code extends from values of the dielectric loss $\epsilon'' = 200$ (red) to $\epsilon'' = 2$ (blue).

are visible, but no abrupt anomalies at the phase transition temperatures can be detected. At the temperature $T_{\mathrm{RE}} = 7$ K magnetic ordering of the Tb ions takes place. The effects of the magnetic and ferroelectric phase transitions on the FIR spectra become evident when zooming into the low-frequency region between 50 and 150 cm^{-1}, which is shown in Figure 4.

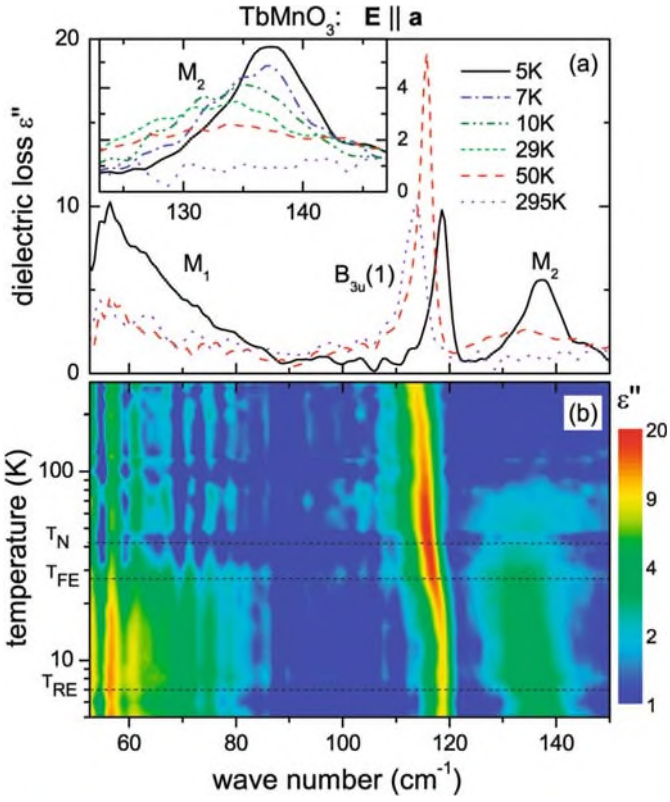

Fig. 4. (Color online) (a) Upper panel: dielectric loss of $TbMnO_3$ for **E** ∥ **a** between 50 and 150 cm^{-1} at a series of temperatures as indicated in the figure. The modes M_1 and M_2 are magnetic excitations. Mode $B_{3u}(1)$ is the phonon mode which couples most strongly to the magnetic excitations. The inset shows the evolution of M_2 with temperature. (b) Color coded contour plot of the dielectric loss as function of temperature and wave number for the same range of frequencies. The color code follows a logarithmic scale and spans the range between 1 (blue) and 20 (red).

The excitations M_1 and M_2 appearing close to 60 and 140 cm^{-1}, respectively, emerge and gain optical weight only below about 40 K (see Fig. 4b), although some diffusive bands seem to persist to higher temperatures. For M_2 this behavior is documented in the inset of Figure 4a. Therefore, these modes are associated with the onset of magnetic ordering at $T_{\mathrm{N}} = 42$ K. In contrast, all phonon modes and here especially $B_{3u}(1)$ show finite optical weight up to room temperature. Recently, the excitation M_1 has been identified as an electromagnon, i.e. an electric-dipole active excitation of a single zone boundary magnon [17]. Note that several electric-dipole active electromagnons and magnetic-dipole active antiferromagnetic resonances have been observed by Pimenov et al. in the frequency region below 25 cm^{-1} in $TbMnO_3$ using THz spectroscopy [9,18].

To date the nature and origin of M_2 remain unsettled. It has been argued that this excitation is due to a two-magnon process (M_1+M_1) with an energy corresponding to the upper cut-off of the magnon density of states [15]. Recently, this scenario has been discarded in

favor of an isotropic Heisenberg-coupling mechanism between non-collinear spins which allows to explain that electromagnons occur only for **E** ∥ **a** [17]. A further possibility is an excitation of the crystal-field split ground state of the $4f$ electrons of the Tb ions. However, the relation to the experimentally observed temperature dependence and to the magnetic ordering of the Mn ions is not in favor of such an interpretation. When looking at the temperature evolution of the lowest-lying phonon $B_{3u}(1)$ close to 120 cm^{-1}, one recognizes that upon entering into the ferroelectric phase below $T_{FE} = 27$ K the phonon shifts and loses intensity (see Figs. 4a and 4b) in agreement with reference [15]. It is this mode which reportedly transfers optical weight to the electromagnons in $GdMnO_3$ [14]. Turning again to Figure 4 it seems that both $B_{3u}(1)$ and M_2 shift to slightly higher frequencies below T_{FE}, but the difference $\Delta\omega = \omega_{M_2} - \omega_{B_{3u}(1)} \cong 20$ cm^{-1} remains almost constant and in agreement with the direct excitation energy of the low-energy electromagnon and antiferromagnetic resonances at 20 cm^{-1} [9,18]. Thus, we suggest to consider the possibility that M_2 could arise from a one-magnon+one-phonon process (1M1P). Multi-magnon plus phonon processes have been described in detail in antiferromagnetic Cu and Ni oxides [31], however, only excitations of even numbers of magnons will yield considerable spectral weight and conserve the total spin. If 1M1P excitations should be realized in $TbMnO_3$, spin-orbit coupling and antisymmetric Dzyaloshinsky-Moriya-like spin coupling ought to contribute to the effective spin-dependent electric-dipole moment.

For a more quantitative analysis of the phonon modes we analyzed all spectra utilizing a 3-parameter fit as outlined above. Table 1 shows eigenfrequencies ω_0 for both polarization directions at room temperature and also indicates the experimentally observed dipole strengths $\Delta\epsilon$ and calculated effective ionic plasma frequencies Ω, which directly provide a measure of the effective dynamic charge involved in a given mode. The effective ionic plasma frequency of all modes, which characterizes the ionicity of the bonds amounts to approximately 1100 cm^{-1}. It has to be compared with the effective ionic plasma frequency $\Omega = 2100$ cm^{-1}, which results from a model assuming ideal ionic bonds (see e.g. Ref. [27]). Let us now turn to the polarization **E** ∥ **a**, the polarization in which the electromagnons show up. Figure 5 documents the temperature dependence of eigenfrequency ω, damping constant γ and dielectric strength $\Delta\epsilon$ of phonon modes $B_{3u}(i)$ with $i = 1, 2, 4$.

Looking now at mode $B_{3u}(1)$ which seems to be most strongly coupled to spin excitations we find the following temperature dependence: coming from room temperature its eigenfrequency (Fig. 5a) reveals the usual hardening due to anharmonicity and starts to saturate below 100 K. We tentatively ascribe this temperature scale to the Curie-Weiss temperature of the manganese subsystem, because in spinel systems spin-phonon coupling effects became evident below the corresponding Curie-Weiss temperatures [32–37]. Moreover the temperature scale of 100 K agrees well with the Curie-Weiss temperature of

Table 1. Phonon eigenfrequencies ω_0, ionic plasma frequencies Ω and dipolar strengths $\Delta\epsilon$ of all 7 B_{1u} and 9 B_{3u} modes in $TbMnO_3$ at room temperature.

B_{1u}	7 Phonons		
Mode	ω_0 (cm^{-1})	Ω (cm^{-1})	$\Delta\epsilon$
1	169.5	301.7	3.19
2	186.7	233.5	1.54
3	335.4	176.5	0.35
4	377.7	395.1	1.09
5	384.9	705.4	3.44
6	580.4	589.0	0.99
7	644.4	168.4	0.07
Σ		1098	10.67
B_{3u}	9 Phonons		
Mode	ω_0 (cm^{-1})	Ω (cm^{-1})	$\Delta\epsilon$
1	113.7	60.7	0.28
2	186.7	319.9	2.94
3	225.0	494.9	4.84
4	307.0	145.6	0.22
5	327.4	257.1	0.62
6	401.8	467.4	1.35
7	466.5	569.0	1.49
8	513.9	76.8	0.02
9	567.7	550.1	0.94
Σ		1135	12.7

$LaMnO_3$ [38]. But on further cooling and passing the magnetic phase transitions the eigenfrequency suddenly increases further. Experimentally, it seems that the increase starts already below the first antiferromagnetic phase transition where collinear spin order is established and further increases when passing the phase transition into a ferroelectric ground state and helical spin order. In total, this increase due to the onset of AFM order amounts to 3% indicating strong spin-phonon coupling. The damping (Fig. 5b) continuously decreases without significant traces of the magnetic and ferroelectric phase transitions. Finally, the most striking effects show up in the temperature dependence of the dielectric strength (Fig. 5c). Starting from room temperature, the strength slightly increases but significantly decreases below the onset of AFM and FE order. The decrease below T_N amounts to more than 50%. It is clear that this effect does not result from the change in the eigenfrequency, but must be directly related to severe changes of the ionic plasma frequency which directly is related to the effective charges involved in the specific phonon mode.

Further representative examples for the temperature dependencies of phonon excitations are shown in Figure 5, documenting the temperature dependencies of the fitting parameters for $B_{3u}(2)$ (Figs. 5d–5f) and $B_{3u}(4)$ (Figs. 5g–5i). $B_{3u}(2)$ exhibits a temperature dependence of the eigenfrequency which is close to what is expected for a purely anharmonic behavior. However, the damping

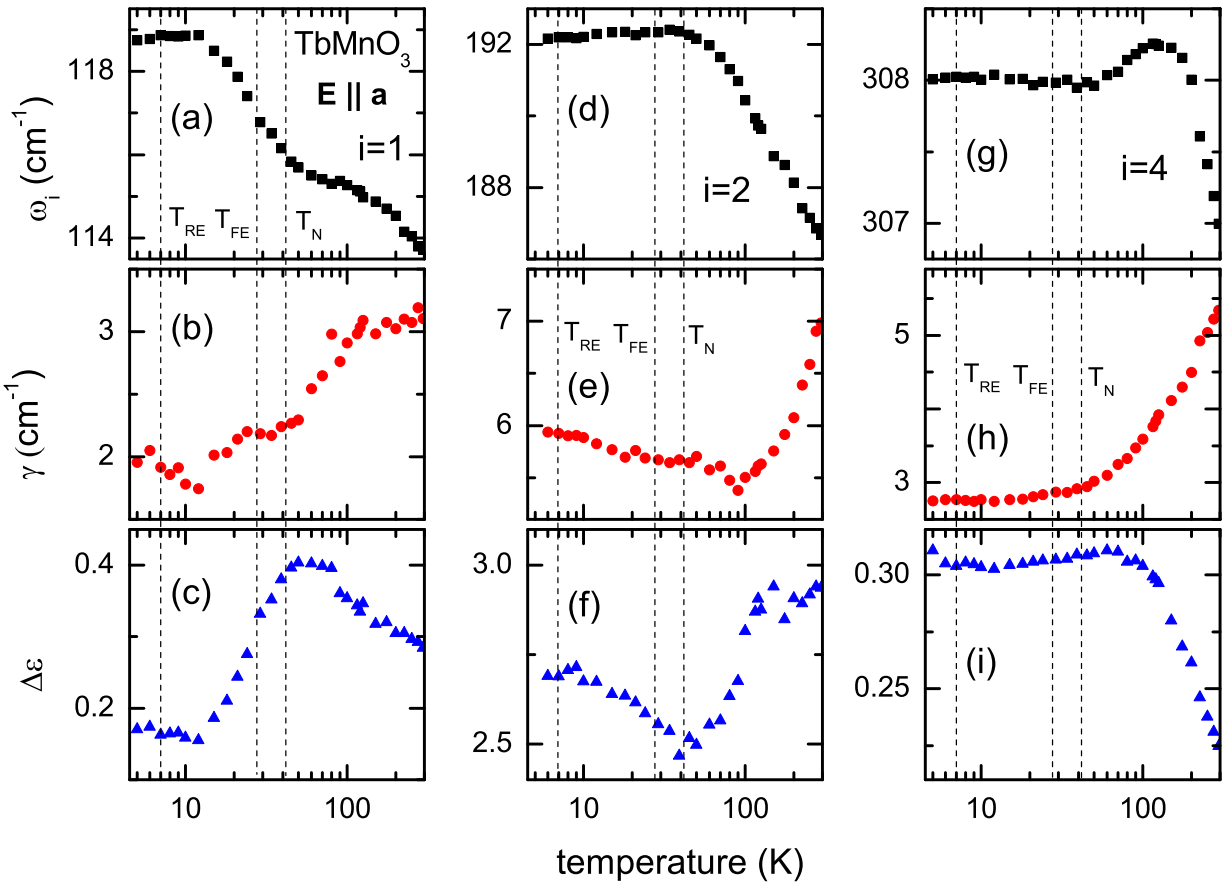

Fig. 5. (Color online) Temperature dependencies of eigenfrequency (a, d, g), damping constant (b, e, h) and dielectric strength (c, f, i) for modes $B_{3u}(i)$ ($i = 1, 2, 4$) in $TbMnO_3$ for $\mathbf{E} \parallel \mathbf{a}$ on semilogarithmic scale. The magnetic ordering temperatures are indicated by vertical dashed lines.

reveals a slight increase below 100 K. The dielectric strength decreases below 100 K and starts to increase again below the onset of AFM order. In contrast, mode $B_{3u}(4)$ decreases in eigenfrequency below 100 K (Fig. 5g), a rather "normal" anharmonic temperature dependence of the damping constant (Fig. 5h) and on cooling from room temperature an unexpected and large increase of the polar strength up to 100 K (Fig. 5i). From this figure it becomes clear that there is no common behavior, but instead eigenfrequencies, damping constants and polar strengths are different for each mode. A specific phonon mode involves specific bonds of neighboring ions which obviously are differently influenced by magnetic exchange as well as magnetoelectric interactions.

Similar observations can also be made for phonon excitations for $\mathbf{E} \parallel \mathbf{c}$. Representative examples are documented in Figure 6, where the left frames show the relevant fitting parameters of mode $B_{1u}(1)$ (Figs. 6a–6c) and the right frames those of mode $B_{1u}(2)$ (Figs. 6d–6f). Here, on decreasing temperature, both eigenfrequencies reveal a decrease below 100 K, but the observed dipolar strengths of these two modes behave drastically different: on cooling we determined an increase of mode $B_{1u}(1)$ (Fig. 6c), but a decrease for mode $B_{1u}(2)$ (Fig. 6f). The effects amount in both cases to more than 10% and seem not to be directly related to the AFM or FE phase transitions. They start at about 100 K, clearly above the appearance of any magnetic or polar order.

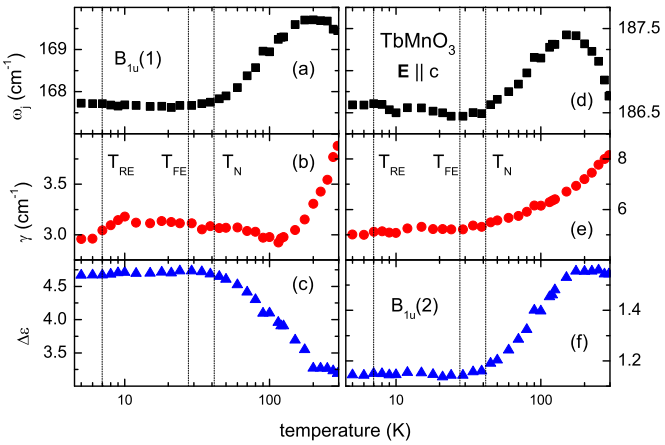

Fig. 6. (Color online) Temperature dependencies of eigenfrequency, damping constant and mode strength for modes $B_{1u}(1)$ and $B_{1u}(2)$ in $TbMnO_3$ for $\mathbf{E} \parallel \mathbf{c}$ on semilogarithmic plots. The magnetic ordering temperatures are indicated by vertical dashed lines.

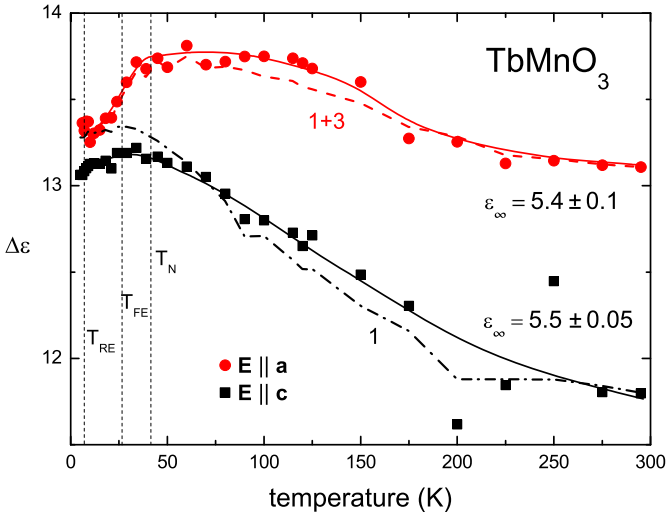

Fig. 7. (Color online) Temperature dependencies of the ionic contribution to the dielectric constant in $TbMnO_3$ for $\mathbf{E} \parallel \mathbf{a}$ (red dots) and $\mathbf{E} \parallel \mathbf{c}$ (black squares). The magnetic ordering temperatures are indicated by vertical dashed lines. The electronic contributions to the dielectric constant are also indicated. Solid lines are drawn to guide the eye. The sum of $\Delta\epsilon$ from modes $B_{3u}(1)$ and $B_{3u}(2)$ for $\mathbf{E} \parallel \mathbf{a}$ is indicated as red dashed line. $\Delta\epsilon$ of mode $B_{1u}(1)$ for $\mathbf{E} \parallel \mathbf{c}$ is indicated as black dash-dotted line. Both contributions have been shifted by a constant offset to agree with the values of the total dipolar strengths at room temperature.

Finally, we discuss the total strength of all polar active modes as documented in Table 1, in order to determine the overall temperature dependence of the dielectric constants along the crystallographic **a** and **c** directions. Here, we summed over all modes. The temperature dependence of the total polar strength is shown in Figure 7. For $\mathbf{E} \parallel \mathbf{a}$ the polar strength slightly increases and considerably drops below the AFM and FE transition. This behavior provides experimental evidence that optical weight is transferred from the phonon excitations to the electromagnons at lower wave numbers, which have not been treated explicitly in the present work. It seems clear that the growing intensity of the electromagnons just compensates for the loss of dipolar strength of the phonon modes. A closer inspection of the temperature dependencies of all 9 B_{3u} modes documents that this transfer of optical weight at the onset of non-collinear spin order mainly results from mode $B_{3u}(1)$ ($\Delta\epsilon = -0.25$; see Fig. 5c) and mode $B_{3u}(3)$ ($\Delta\epsilon = -0.25$; not shown). It is interesting to note, that in clear contradiction to this behavior, phonon mode $B_{3u}(2)$ gains strength at low temperatures ($\Delta\epsilon = 0.2$; see Fig. 5f). It would be highly interesting to find out, if in the latter case the transferred optical strength comes from spin waves via magnetoelectric interactions.

To document the fact that the temperature dependence of the dielectric constant in $TbMnO_3$ for $\mathbf{E} \parallel \mathbf{a}$ mainly results from the modes $B_{3u}(1)$ and $B_{3u}(3)$, the sum of the dipolar strength of these two modes is indicated in Figure 7 by the red dashed line and has been shifted by an offset to agree with the total dipolar strength of all modes at room temperature. This representation nicely demonstrates that these two modes lose intensity below the onset of spiral spin order.

Most eigenfrequencies for $\mathbf{E} \parallel \mathbf{a}$ reveal rather normal anharmonic behavior, with a smooth increase of the order of 1 or 2 cm^{-1} on cooling. Significant spin-phonon coupling below the onset of magnetic order only becomes apparent for mode $B_{3u}(1)$, as documented in Figure 4a. An unexpected temperature dependence of the transverse optical modes has been deduced for modes $B_{3u}(i)$ with $i = 6, 7, 8$: in all cases the eigenfrequencies pass through a maximum roughly located at 100 K and decrease on further cooling. This decrease amounts to 2 cm^{-1} for $B_{3u}(6)$ and approximately 1 cm^{-1} for modes $B_{3u}(7)$ and $B_{3u}(8)$ (not shown).

As shown in Figure 7, for $\mathbf{E} \parallel \mathbf{c}$ the total polar strength of all phonons and concomitantly the dielectric constant shows a significant increase towards low temperatures and saturates below 100 K. No significant anomalies are observed on passing the magnetic phase transitions. The increase of polar weight for $T > 100$ K mainly results from mode $B_{1u}(1)$ ($\Delta\epsilon = 1.5$; see Fig. 6c). This is indicated by the dash-dotted line which indicates the dielectric strength of this mode and has been shifted to coincide with the sum over all dipolar strengths for this direction at room temperature.

The almost constant total weight at low temperatures (Fig. 7) corresponds to the absence of transfer of optical weight to spin excitations. Indeed, electromagnons in multiferroic rare earth manganites only appear with polarization $\mathbf{E} \parallel \mathbf{a}$.

For $\mathbf{E} \parallel \mathbf{c}$, most eigenfrequencies exhibit rather canonical anharmonic behavior, with the exception of modes $B_{1u}(1)$ and $B_{1u}(2)$ (see Figs. 6a and 6d). For these modes the eigenfrequencies pass through maxima at enhanced temperatures and decrease on further cooling. No anomalies show up at the magnetic transitions.

The total dielectric constant is the sum of all $\Delta\epsilon$ plus the electronic contribution. We determined the electronic dielectric constant ϵ_∞ from fits to the reflectivity as function of temperature up to 4 000 cm^{-1} independently for both directions. We found no significant temperature dependence and arrived at estimates for ϵ_∞ as 5.4 for $\mathbf{E} \parallel \mathbf{a}$ and 5.5 for $\mathbf{E} \parallel \mathbf{c}$.

This gives estimates of the dielectric constants of 18.7 for $\mathbf{E} \parallel \mathbf{a}$ and 18.6 for $\mathbf{E} \parallel \mathbf{c}$ at low temperatures. One should have in mind that the dielectric constant for $\mathbf{E} \parallel \mathbf{a}$ does not include the contribution of the electromagnon. For $\mathbf{E} \parallel \mathbf{a}$ this result seems to be compatible with published values of measurements at lower frequencies: Kimura [1] and Pimenov [9] reported a dielectric constant $\epsilon = 24$ as measured at audio or GHz frequencies respectively. If we assume that most of the weight from the 120 cm^{-1} phonon excitation is transferred to the 60 cm^{-1} electromagnon (see e.g. Ref. [17]), according to Figure 6 we can estimate the contribution of the electromagnon to the low-frequency dielectric constant to be of the order of 2 and there seems reasonable agreement between our high-frequency and the low-frequency results. For $\mathbf{E} \parallel \mathbf{c}$,

Kimura reported values of 29 [1] or 23.5 [24], both values are considerably enhanced compared to our result.

4 Summary

Using FIR spectroscopy we studied in detail the phonon excitations for $\mathbf{E} \parallel \mathbf{a}$ and $\mathbf{E} \parallel \mathbf{c}$ and their coupling to the magnetic degrees of freedom of multiferroic $TbMnO_3$. The main results can be summarized as follows:

(i) All nine B_{3u} modes expected for $\mathbf{E} \parallel \mathbf{a}$ and the seven B_{1u} modes expected for $\mathbf{E} \parallel \mathbf{c}$ were assigned and listed in Table 1. Almost all phonon modes reveal anomalies in their eigenfrequencies, damping constants or ionic strengths. Most of these anomalies appear at the magnetic and FE phase transitions indicating magnetoelectric coupling effects. However, in some cases anomalies appear at significantly higher temperatures of about 100 K and may be linked to the Curie-Weiss temperature by spin-phonon coupling similarly to other systems with magnetic frustration [27,33–36]. The effects in the eigenfrequencies are of the order of 1 to 2 cm^{-1} in agreement with observations in other multiferroics [39,40].

(ii) The difference in frequency $\Delta\omega = \omega_{M_2} - \omega_{B_{3u}(1)} \cong 20\ cm^{-1}$ between the lowest phonon $B_{3u}(1)$ and the mode M_2, which emerges in the magnetically ordered phase, is almost constant with temperature and corresponds to the energy scale of the low-energy electromagnons and antiferromagnetic resonances. This may be an indication of a one-(electro)magnon+one phonon process.

(iii) There is no apparent phonon softening close to the ferroelectric phase transition, an observation which is compatible with the assumption that ferroelectric order is driven by the onset of helical spin order and the ferroelectricity is of improper type.

(iv) There is transfer of spectral weight of phonons with $\mathbf{E} \parallel \mathbf{a}$ to electromagnon excitations, i.e. spin waves which gain polar weight through strong magnetoelectric coupling (see Fig. 4b). In total this transfer of dielectric strength corresponds to a decrease of the dielectric constant just below the phonon frequencies of approximately 0.5 (see Fig. 7).

(v) Unexpectedly, we observed a significant increase of the dielectric constant for $\mathbf{E} \parallel \mathbf{c}$ which results from an increase of the effective ionic plasma frequency on cooling. This observation could be a characteristic scenario for spin-driven ferroelectrics. While in displacive ferroelectrics polar order is established by a continuous softening of a transverse optical phonon mode with a concomitant increase of the static dielectric constant, it seems that in the spin-driven improper ferroelectrics an increase of the dielectric constant follows from an increase of dynamical charges indicating charge transfer processes. Recent density functional theory [41,42] and first principal calculations [43] stress the importance of conventional polar atomic displacements, but also demonstrate the importance of purely electronic contributions to the polarization, which results from a spin-orbit interaction modifying the hybridization of electronic orbitals [5].

We acknowledge fruitful discussions with A. Pimenov and Th. Kopp. This research was supported by the Deutsche Forschungsgemeinschaft (DFG) via the Collaborative Research Center, SFB484 (Augsburg).

References

1. T. Kimura, T. Goto, H. Shintani, K. Ishizaka, T. Arima, Y. Tokura, Nature **426**, 55 (2003)
2. M. Fiebig, J. Phys. D: Appl. Phys. **38**, R123 (2005)
3. S.W. Cheong, M. Mostovoy, Nat. Mater. **6**, 13 (2007)
4. R. Ramesh, N.A. Spaldin, Nat. Mater. **6**, 21 (2007)
5. H. Katsura, N. Nagaosa, A. Balatsky, Phys. Rev. Lett. **95**, 057205 (2005)
6. M. Mostovoy, Phys. Rev. Lett. **96**, 067601 (2006)
7. I. Sergienko, E. Dagotto, Phys. Rev. B **73**, 094434 (2006)
8. G.A. Smolenskii, I.E. Chupis, Sov. Phys. Usp. **25**, 475 (1982)
9. A. Pimenov, A. Mukhin, V. Ivanov, V. Travkin, A. Balbashov, A. Loidl, Nat. Phys. **2**, 97 (2006)
10. A.B. Sushkov, R.V. Aguilar, S.W. Cheong, H.D. Drew, Phys. Rev. Lett. **98**, 027202 (2007)
11. R.V. Aguilar, A.B. Sushkov, C.L. Zhang, Y.J. Choi, S.W. Cheong, H.D. Drew, Phys. Rev. B **76**, 060404 (2007)
12. A. Pimenov, A. Loidl, A.A. Mukhin, V.D. Travkin, V.Y. Ivanov, A.M. Balbashov, Phys. Rev. B **77**, 014438 (2008)
13. A.B. Sushkov, M. Mostovoy, R.V. Aguilar, S.W. Cheong, H.D. Drew, J. Phys.: Condens. Matter **20**, 434210 (2008)
14. A. Pimenov, A.M. Shuvaev, A.A. Mukhin, A. Loidl, J. Phys.: Condens. Matter **20**, 434209 (2008)
15. Y. Takahashi, N. Kida, Y. Yamasaki, J. Fujioka, T. Arima, R. Shimano, S. Miyahara, M. Mochizuki, N. Furukawa, Y. Tokura, Phys. Rev. Lett. **101**, 187201 (2008)
16. N. Kida, Y. Yamasak, R. Shimano, T.H. Arima, Y. Tokura, J. Phys. Soc. Jpn **77**, 123704 (2008)
17. R.V. Aguilar, M. Mostovoy, A.B. Sushkov, C.L. Zhang, Y.J. Choi, S.W. Cheong, H.D. Drew, Phys. Rev. Lett. **102**, 047203 (2009)
18. A. Pimenov, A. Shuvaev, A. Loidl, F. Schrettle, A.A. Mukhin, V.D. Travkin, V.Y. Ivanov, A.M. Balbashov, Phys. Rev. Lett. **102**, 107203 (2009)
19. A. Pimenov, T. Rudolf, F. Mayr, A. Loidl, A.A. Mukhin, A.M. Balbashov, Phys. Rev. B **74**, 100403 (2006)
20. M. Kenzelmann, A. Harris, S. Jonas, C. Broholm, J. Schefer, S. Kim, C. Zhang, S. Cheong, O. Vajk, J. Lynn, Phys. Rev. Lett. **95**, 087206 (2005)
21. H. Katsura, A.V. Balatsky, N. Nagaosa, Phys. Rev. Lett. **98**, 027203 (2007)
22. D. Senff, P. Link, K. Hradil, A. Hiess, L.P. Regnault, Y. Sidis, N. Aliouane, D.N. Argyriou, M. Braden, Phys. Rev. Lett. **98**, 137206 (2007)
23. D. Senff, N. Aliouane, D.N. Argyriou, A. Hiess, L.P. Regnault, P. Link, K. Hradil, Y. Sidis, M. Braden, J. Phys.: Condens. Matter **20**, 434212 (2008)
24. T. Kimura, G. Lawes, T. Goto, Y. Tokura, A. Ramirez, Phys. Rev. B **71**, 224425 (2005)
25. A.B. Kuzmenko, Rev. Sci. Instrum. **76**, 083108 (2005)

26. Note that the excitation M_1 was not included in the fit routine, because it is very close to the experimental low-frequency limit and a band-fourier-filter was used to smoothen the interference fringes superimposed on the spectra due to multiple reflections in the sample.
27. T. Rudolf, C. Kant, F. Mayr, J. Hemberger, V. Tsurkan, A. Loidl, Phys. Rev. B **76**, 174307 (2007)
28. K. Yamauchi, S. Picozzi, J. Phys.: Condens. Matter **21**, 064203 (2009)
29. K. Tobe, T. Kimura, Y. Okimoto, Y. Tokura, Phys. Rev. B **64**, 184421 (2001)
30. N. Kovaleva, A. Boris, C. Bernhard, A. Kulakov, A. Pimenov, A. Balbashov, G. Khaliullin, B. Keimer, Phys. Rev. Lett. **93**, 147204 (2004)
31. J. Lorenzana, G. Sawatzky, Phys. Rev. B **52**, 9576 (1995)
32. A. Sushkov, O. Tchernyshyov, W. Ratcliff, S. Cheong, H. Drew, Phys. Rev. Lett. **94**, 137202 (2005)
33. T. Rudolf, C. Kant, F. Mayr, J. Hemberger, V. Tsurkan, A. Loidl, Phys. Rev. B **75**, 052410 (2007)
34. J. Hemberger, T. Rudolf, H.A.K. von Nidda, F. Mayr, A. Pimenov, V. Tsurkan, A. Loidl, Phys. Rev. Lett. **97**, 087204 (2006)
35. J. Hemberger, H.A.K. von Nidda, V. Tsurkan, A. Loidl, Phys. Rev. Lett. **98**, 147203 (2007)
36. T. Rudolf, C. Kant, F. Mayr, J. Hemberger, V. Tsurkan, A. Loidl, New J. Phys. **9**, 76 (2007)
37. T. Rudolf, C. Kant, F. Mayr, M. Schmidt, V. Tsurkan, J. Deisenhofer, A. Loidl, Eur. Phys. J. B **68**, 153 (2009)
38. M. Paraskevopoulos, F. Mayr, J. Hemberger, A. Loidl, R. Heichele, D. Maurer, V. Muller, A. Mukhin, A. Balbashov, J. Phys.: Condens. Matter **12**, 3993 (2000)
39. R.V. Aguilar, A.B. Sushkov, S. Park, S.W. Cheong, H.D. Drew, Phys. Rev. B **74**, 184404 (2006)
40. A.F. Garcia-Flores, E. Granado, H. Martinho, C. Rettori, E.I. Golovenchits, V.A. Sanina, S.B. Oseroff, S. Park, S.W. Cheong, J. Appl. Phys. **101**, 09M106 (2007)
41. H.J. Xiang, S.H. Wei, M.H. Whangbo, J.L.F. Da Silva, Phys. Rev. Lett. **101**, 037209 (2008)
42. A. Malashevich, D. Vanderbilt, Phys. Rev. Lett. **101**, 037210 (2008)
43. S. Picozzi, K. Yamauchi, B. Sanyal, I.A. Sergienko, E. Dagotto, Phys. Rev. Lett. **99**, 227201 (2007)